J. Min. Metall. Sect. B-Metall. 50 (1) B (2014) 31 - 36

Journal of Mining and Metallurgy, Section B: Metallurgy

APPLICATION OF SACRIFICIAL COATINGS AND EFFECT OF COMPOSITION ON Al-Al_3Ni ULTRAFINE EUTECTIC FORMATION

L. Čelko[a, b,*], L. Klakurková[a, b], B. Smetana[c], K. Slámečka[a, b], M. Žaludová[c], D. Hui[d], J. Švejcar[a, b]

[a] Brno University of Technology, CEITEC - Central European Institute of Technology, Brno, Czech Republic
[b] Brno University of Technology, Faculty of Mechanical Engineering, Brno, Czech Republic
[c] Technical University of Ostrava, Faculty of Metallurgy and Materials Engineering, Ostrava, Czech Republic
[d] University of New Orleans, Department of Mechanical Engineering, New Orleans, USA

(Received 13 October 2012; accepted 06 December 2013)

Abstract

This paper introduces an unconventional method designed for forming hypereutectic alloys via coating deposition onto the substrate surface and subsequent heat treatment of such systems. The coating was produced from 99.7 wt% nickel powder by means of high velocity oxyfuel (HVOF) spraying onto the surface of 99.999 wt% aluminium sheet. The specimens were manufactured immediately after the spraying. Specimens were heat-treated using a differential thermal analysis (DTA) apparatus up to a temperature of 900°C and then cooled down to the room temperature in an argon atmosphere with constant heating and cooling rates, under which the $NiAl_3$ intermetallic phase formed within the initial substrate. Two different alloy microstructures consisting of a coarse eutectic and an ultrafine well-dispersed eutectic were produced. The formation processes and resultant microstructures were studied by means of differential thermal analysis, metallography, scanning electron microscopy, energy dispersive microanalysis, and image analysis techniques.

Keywords: *Aluminium alloys, aluminides miscellaneous, plasma spraying, differential thermal analysis, scanning electron microscopy*

1. Introduction

The history of manufacturing pure aluminium begins in 1825, when the Danish experimenter Hans Christian Oested made a few small buttons of silver-like metal from bauxite by a chemical method. Nowadays, it is hard to imagine that despite the fact that aluminium is the third most common element in the earth crust and bauxite as a raw material contains almost 8.5% of it, the cost of pure aluminium prepared in this way was comparable to the price of platinum. After its discovery, aluminium was widely used in jewellery for the next almost 50 years until Charles Martin Hall in USA and Paul Herault in France independently discovered in 1886 the electro-chemical process (currently known as the Hall-Herault process) of its production, which introduced aluminium into industry and enabled its usage in a broad range of engineering applications [1].

Currently, aluminium alloys are widely used in many components and structural parts across the industries, mostly due to their very low density, excellent oxidation resistance provided by formed thin alumina (Al_2O_3) layer and good workability. The aerospace, aircraft, automotive, food-processing and building industries can be mentioned as some of the most prominent application examples [2,3]. However, in spite of aforementioned positives, the usability of aluminium alloys is often limited by their rather poor mechanical resistance in comparison to other metals, which led to the development of several methods aimed at improving their mechanical properties. One group of these methods is based on the formation of a composite alloy by introducing metallic, intermetallic or ceramic second-phase particles with high elastic modules [4,5]. Other methods are based on complex heat treatments [6-8] and on optimizing (specific) the alloy forming process (forging, superplastic forming) [9-11]. In the case of strengthening by intermetallics, the eutectic reaction can easily be utilized. Depending on the concentration of constituents, hypo-eutectic, (near) eutectic or hyper-eutectic alloys could be produced [12-14].

* *Corresponding author: ladislav.celko@ceitec.vutbr.cz*

DOI:10.2298/JMMB121013038C

In this paper, a new unconventional method consisting in forming a sacrificial nickel coating on aluminium substrate and its subsequent annealing at temperatures above the melting point of aluminium has been used to produce hypereutectic aluminium alloys. The formation processes and resultant microstructures were studied by means of differential thermal analysis, metallography, scanning electron microscopy, energy dispersive microanalysis, and image analysis techniques.

2. Experimental

2.1 Experimental Material

A sheet of 99.999 wt% Al (Al Invest Inc., Czech Republic) was used as the substrate. The sheet surface was ground with abrasive paper #600, etched with the Tucker solution (45 ml HCl + 15 ml HNO_3 + 15 ml HF + 25 ml H_2O) and washed with acetone in an ultrasonic cleaning bath with the aim of disrupting the oxide layer and degreasing the sheet surface before coating deposition. The 99.7 wt% was sprayed onto the sheet surface using the High Velocity OxyFuel technique (HVOF). The carrier gas mixture of propane (40 L/min), oxygen (160 L/min) and nitrogen (3.2 L/min) was used during HVOF spraying. The average as-sprayed coating thickness was about 125 μm. After spraying, samples of 2.5 × 2.5 × approx. 0.5 mm in size were cut out from the Ni-coated side of the Al sheet. To ensure a uniform weight, the thickness of specimens was reduced by grinding the aluminium side (the side without the sacrificial nickel coating) with abrasive paper #1000. The resulting weight of specimens was 10.23 mg.

2.2 Experimental Procedure

The differential thermal analysis (DTA) measurements were performed using a Setaram SETSYS-18 DTA facility and alumina crucibles. The temperature was altered between T_L = 20°C and T_H = 900°C with a constant heating and cooling rate of 5°C.min^{-1}.The measuring cell was emptied and refilled with high purity argon (6N) three times prior to the measurements. An argon gas flow of 2 L.h^{-1} was maintained during all tests. The S-type rod PtRh10% thermocouples were used for determining the temperature. Prior to experiments, the thermocouples were calibrated according to the standard [15] by measuring the extrapolated onset temperature of the melting peaks of aluminum (660°C) and nickel (1455°C) standards. The accuracy of the temperature calibration was ± 1°C. Since the temperature calibration during cooling was not performed, the undercooling effects are discussed qualitatively.

2.3 Characterization techniques

Specimens of hypereutectic aluminium alloys selected for microscopic observations were ground by increasingly finer abrasive papers (up to #4000) and subsequently polished with diamond pastes (down to 1 μm) and with the OP-U colloidal silica final suspension (Co. Struers GmbH). Investigations were accomplished by means of the scanning electron microscope (SEM) Philips XL-30 equipped with the energy dispersive X-ray (EDX) spectroscopy microanalyser by the EDAX company. The layer thicknesses and quantity of individual phases were determined based on the SEM images by using the NIS Elements AR 2.3 image analysis software.

3. Results and Discussion

3.1 Initial state

The initial as-sprayed specimens (without any heat treatment) exhibited a microstructure that is typical of HVOF sprayed coatings and cold-rolled aluminium sheets, Fig 1. The as-sprayed coating consists of nickel splats (around 92%), voids and oxide particles that are located at triple points and in between the splats. The amount of voids and oxides is

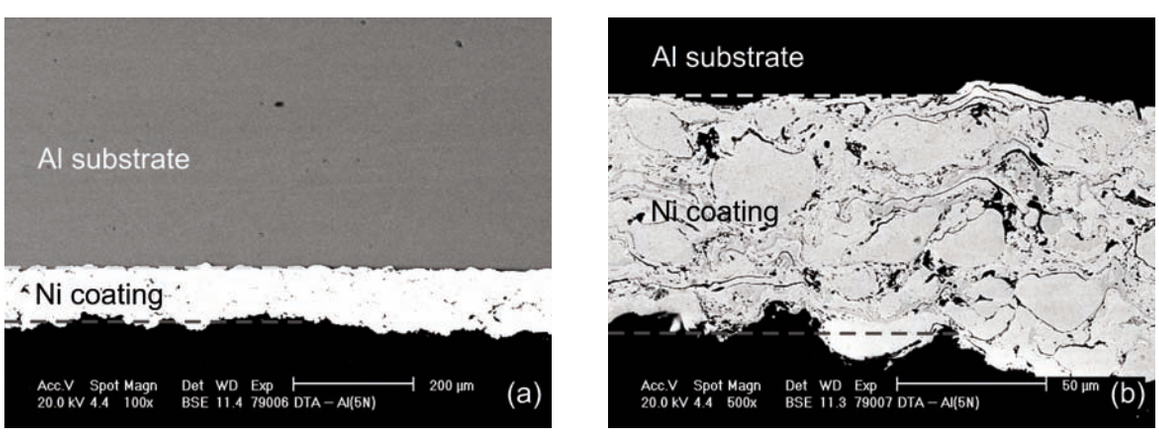

Figure 1. SEM micrographs of initial-state microstructure: (a) HVOF sprayed nickel coating on aluminium substrate, (b) detail of coating-substrate interface.

approximately 8%, which is rather large when compared with the 1-2% commonly reported for the HVOF technique in the literature [16]. The larger amount of oxides presumably arose from utilized deposition conditions that had to be chosen experimentally due to the absence of recommendations from the manufacturer of the nickel powder. The microstructure of the substrate was typical of cold-rolled aluminium sheets with a small amount (less than 1%) of pores. As expected, the interface between the aluminium sheet substrate and the HVOF nickel coating was sharp and without any apparent mutual interactions.

3.2 DTA investigations

The results of two DTA measurements of nickel coated specimens are shown as Fig 2. The heating and cooling curves were measured during a single heating/cooling cycle. Note that three or more of such cycles are usually used. However, it was found, that more cycles resulted in undesirable coarsening of the intermetallic phase within the eutectic. Because the DTA technique is conventionally used for bulk alloys and not for coated alloy systems, where mutual interactions of diffusing elements result in the formation of intermetallic layers and/or strengthening of particles, the interpretation of the data obtained was more difficult and required experience with the Al-Ni system produced by heat treatment in solid (up to 640°C), semi-solid (in the range of 640 – 660°C) and molten states (above 660°C) [17,18].

For all the investigated specimens, the first deflection of the heating curve from the base line before the melting was observed at 623°C in the exothermic direction. Based on our previous work in this temperature region [17], this reaction was related to an intensive diffusion that results in the formation of continuous Ni_2Al_3 and $NiAl_3$ (neighbouring intermetallic phases in Al-Ni phase diagram [19]) layers along the initial coating-substrate interface. Following this reaction, the melting at a temperature 640°C was observed corresponding clearly to the melting point of the eutectic in the Al-Ni binary system (639.9°C) [19]. The presence of the nickel coating on the aluminium substrate shifted the melting temperature of pure aluminium (660°C) down to the melting point of the Al-$NiAl_3$ eutectic. When melting occurred, the eutectic consisting of Al and the $NiAl_3$ phase starts to form. The area of endothermic melting reaction slightly differed for individual specimens. As the weight of all specimens was the same, this effect was probably caused by local differences in the initial (after deposition) thickness of nickel coating, which was unavoidable due to the HVOF process constraints. Clearly, due to the different densities of nickel (8.91 $g.cm^{-3}$) and aluminium (2.70 $g.cm^{-3}$), a small variation in the thickness of Ni coating can result in a significantly thinner or thicker Al part of the specimen. In the temperature interval of 655-721°C, where the DTA curve changed from the endothermic to exothermic reaction, further diffusion of nickel from the coating into the aluminium substrate took place and the primary $NiAl_3$ rounded particles in the molten aluminium eutectic start to form. When both heating curves in Fig. 2 are compared, further nickel oversaturation is observed in the temperature range of 721-860°C in alloy I (Fig. 2a). By contrast, the coating was completely dissolved at a temperature of 721°C in the case of alloy II and no further Ni oversaturation is observed, Fig. 2b.

During the cooling of alloy I, the first exothermic effect was found at a temperature of 850°C, at which the coarse primary $NiAl_3$ particles crystallized. Consistently, this effect was not found in alloy II due to the lack of nickel oversaturation in the temperature interval of 721-860°C. The next exothermic effect in alloy I occurred at a temperature of 640°C, where the Al+$NiAl_3$ eutectic started to form. There was no gap apparent between the onset points of eutectic melting (heating curve) and crystallization (cooling curve), Fig 2a, which indicated the pre-existence of a number of nucleation sites in the melt (primary $NiAl_3$ intermetallic phase particles formed at a temperature of 850°C), and a heterogeneous nucleation mechanism of coarse eutectic was expected. In the case of alloy II, it was apparent that the mechanism of eutectic formation differed from that of alloy I, which was also indicated by the gap of approx. 5°C between the onset points of eutectic melting and crystallization. In alloy II, crystallization occurred in two steps, consisting of the formation of primary intermetallic particles in molten aluminium at 671°C and subsequent solidification of the eutectic into an ultrafine and well-dispersed $NiAl_3$ intermetallic phase in aluminium at a temperature of 634°C. In this case, the absence of nucleation sites within the melt enabled the formation of ultrafine eutectic driven by the mechanism of homogeneous nucleation. Generally, there are only a few factors that play a crucial role in the formation of alloys or interconnections. These are especially the temperature applied, the time of processing and the initial composition. As the former two factors were identical for all alloys, the one factor that clearly plays the key role in this case was the slight difference in the initial composition. This explanation seems to be supported by experiments on Ni/Al/Ni interconnections with thin Al layers. Annealing such systems at a temperature of 720°C, which was found in this study to correspond to ultrafine eutectic formation, resulted in a microstructure consisting of NiAl, Ni-rich NiAl and Ni_3Al (Ni-rich nickel aluminide intermetallics from the opposite site of the Al-Ni binary system) [19, 20]. Similar microstructures containing Ni-rich

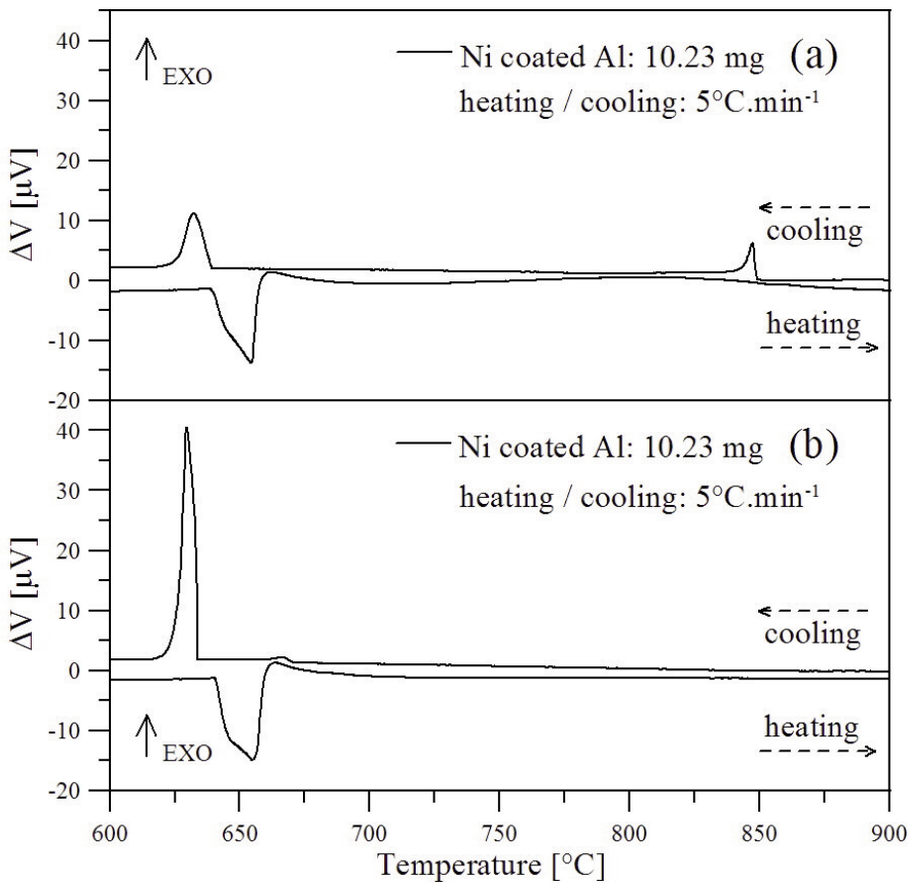

Figure 2. DTA plots of heating and cooling curves of: (a) alloy I – coarse eutectic hypereutectic alloy, (b) alloy II – ultrafine eutectic hypereutectic alloy.

intermetallics were created also by varying the other two aforementioned factors, i.e. by increasing the temperature and shortening the processing time [21, 22].

3.3 Microstructural characterization

Depending on the differences in DTA data, the microstructure of sacrificial nickel coated specimens after the heat treatment differed due to the variation in the coating thickness. The microstructure of alloy I consisted of a coarse eutectic and coarse primary intermetallic particles (Fig. 3a), while the microstructure of alloy II was composed of an ultrafine, well-dispersed eutectic and a coarse, rounded primary intermetallic phase (Fig. 3b). The microstructure of alloy I (coarse eutectic) was similar to the microstructures of a cast eutectic Al-8.5Ni alloy [4] and of Al-Ni cast alloys produced in last few decades [23, 24]. On the other hand, the microstructure of alloy II (ultrafine eutectic in Al-Ni binary system) produced in this study was unique and to the best of authors' knowledge has not been yet reported in the literature, although there are several studies describing an ultrafine eutectic in other eutectic systems, such as Fe-Si [25], Cr-Si [26] or Ti-Fe-V [27]. Clearly, the initial HVOF sprayed nickel coating was completely dissolved in the molten aluminium substrate, while the intermetallic layers along the original coating-substrate interface, which were found in previous studies at 630°C [17, 18], were not present.

Table 1 summarizes the results of EDX measurements carried out at points designated in Fig. 3. Based on the phase stoichiometry of intermetallic phases in the Al-Ni binary system [19], both produced alloys consisted of the primary $NiAl_3$ intermetallic phase and the $Al+NiAl_3$ eutectic. In the ultrafine eutectic alloy II, the EDX area analyses of five randomly selected rectangular regions of 260 μm^2 across the primary $NiAl_3$ intermetallic phase and $Al+NiAl_3$ eutectic in Fig. 3 resulted in a chemical composition of 89-91% Al and 11-9% Ni [wt.%] that reflected the hypereutectic alloy formation. By using the Ni-Al binary system diagram [19] and the lever rule of mixture, the volume fraction of $NiAl_3$ intermetallic phase in the hypereutectic alloy was expected to be in the range of 26-32 wt%.

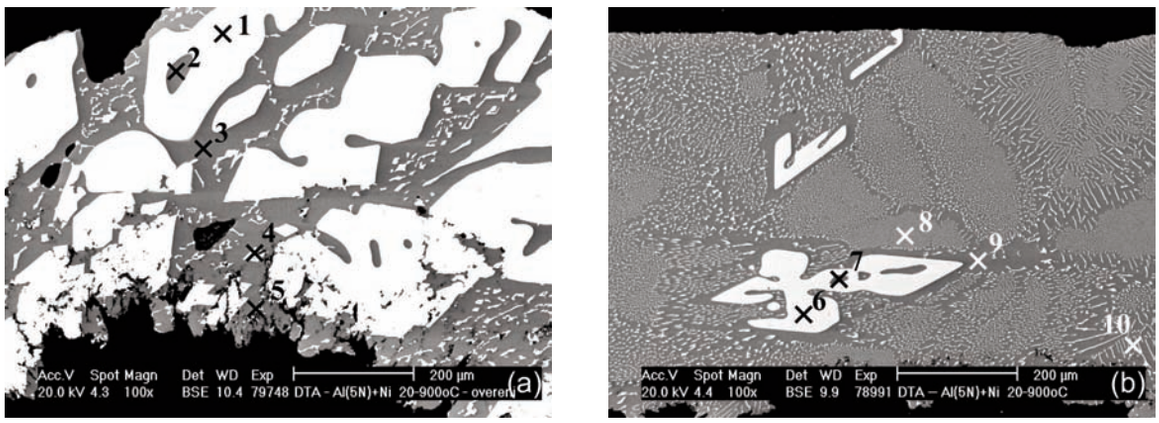

Figure 3. SEM micrographs of (a) alloy I – coarse eutectic hypereutectic alloy, and (b) alloy II – ultrafine eutectic hypereutectic alloy.

Table 1. Chemical composition of produced hypereutectic alloys produced - EDX SEM [wt%] (points from Fig. 3)

Point	Phase	Al	Ni
1	Al_3Ni	75.4	24.6
2	Al	99.4	0.6
3	Al	99.5	0.5
4	Al_3Ni	76.3	23.7
5	Al	100	–
6	Al_3Ni	76.6	23.4
7	Al	100	–
8	(Al)	95	5
9	Al_3Ni	79.8	20.2
10	Al	100	–

In alloy I, the coarse irregular blocks of primary $NiAl_3$ intermetallic phase and coarse Al+$NiAl_3$ eutectic with the length ranging from several tenths to several hundreds of microns were formed during cooling at a temperature of 850°C, DTA data in Fig. 2a, occupying approximately 55% of the initial aluminium substrate volume. On the contrary, the Al+$NiAl_3$ eutectic together with the primary $NiAl_3$ particles occupied only about 28% of the initial aluminium substrate volume in alloy II. The areal fraction of rod-like $NiAl_3$ intermetallic particles in the eutectic was around 22% in the transversal direction (Fig. 4a) and 12% in the longitudinal direction (Fig. 4b) defined with respect to local orientation of the particles in points 8 and 10 (Fig. 3b). Rod-like particles embedded in aluminium were of almost regular circular shape (≈ 0.9 circularity) with 0.2-2.9 µm diameter, 2-65 µm length and the distance between particles ranging from 2 to 10 µm.

4. Conclusion

The designed unconventional two-step method can be utilized for the production of hypereutectic alloys. The initial coating-substrate interface enabled eutectic and primary Al-rich intermetallic phase formation within the aluminium substrate. Heat

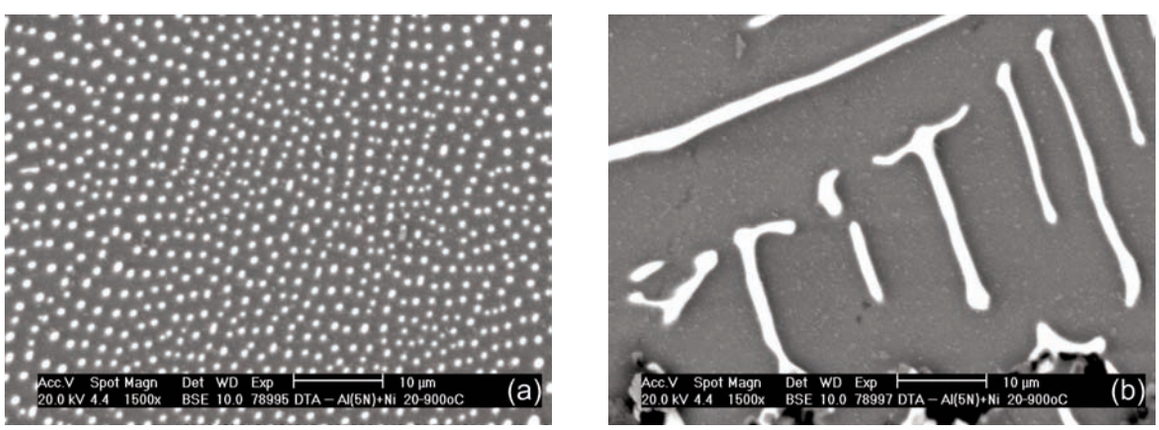

Figure 4. Detailed SEM micrographs of ultrafine eutectic hypereutectic alloy II microstructure in (a) transverse and (b) longitudinal directions, see vicinity of points 8 and 10 in Fig. 3b.

treatment of the aluminium substrate in the molten state did not cause substantial distortion of the initial sheet shape and dimensions. It was found that it is possible to form an ultrafine eutectic in the Al-Ni binary system consisting of aluminium and $NiAl_3$ rod-like intermetallic particles with 0.2-2.9 μm diameter, 2-65 μm length, and the distance between particles ranging from 2 to 10 μm.

Acknowledgements

The authors acknowledge the financial support provided in the frame of the projects (GA7/12/P739) by Czech Science Foundation and "CEITEC – Central European Institute of Technology" (CZ.1.05/1.1.00/02.0068) by European Regional Development Fund.

References

[1] E. Teale, Popular Sci. Monthly, 2 (1936) 25-28.

[2] G.E. Totten, D.S. MacKenzie, Handbook of Aluminium – Vol. 1, Marcel Dekker, New York, 2001.

[3] G.E. Totten, D.S. MacKenzie, Handbook of Aluminium – Vol. 2, Marcel Dekker, New York, 2003.

[4] G. Gonzalez, G.A. Lara-Rodriguez, A. Sandoval-Jiménez, W. Saikaly, A. Charai, Mater. Char., 59 (2008) 1607-1612.

[5] P. Gudlur, A. Forness, J. Lentz, M. Radovic, A. Muliana, Mater. Sci. Eng., 531 A (2012) 18-27.

[6] O.M. Suárez, Mater. Char., 49 (2003) 187-191.

[7] G.F. Li, X.M. Zhang, P.H. Li, J.H. You, Trans. Nonferrous Met. Soc. China, 20 (2010) 935-941.

[8] S. Pogatscher, H. Antrekowitsch, H. Leitner, T. Ebner, P.J. Uggowitzer, Acta Mater., 59 (2011) 3352-3363.

[9] M. Vaseghi, H.S. Kim, Mater. And Design, 36 (2012) 735-740.

[10] V.L. Niranjani, K.C. Kumar, V.S. Sarma, Mater. Sci. Eng., 515 A (2009) 169-174.

[11] I. Nikulin, A. Kipelova, S. Malopheyev, R. Kaibyshev, Acta Mater., 60 (2012) 487-497.

[12] S. Shankar, Y.W. Riddle, M.M. Makhlouf, Acta Mater., 52 (2004) 4447-4460.

[13] H. Bei, E.P. George, G.M. Pharr, Intermetallics, 11 (2003) 283-289.

[14] E.R. Wang, X.D. Hui, G.L. Chen, Mater. And Design, 32 (2011) 4333-4340.

[15] R. Rablbauer, G. Frommeyer, F. Stein, Mater. Sci. Eng., 343 A (2003) 301-307.

[16] L. Pawlowski, The Science and Engineering of Thermal Spray Coatings, Wiley, Chichester, 2008.

[17] L. Čelko, L. Klakurková, J. Švejcar, Defect Diffus. Forum, 297-301 (2010) 771-777.

[18] L. Klakurková, L. Čelko, K. Slámečka, P. Doležal, J. Švejcar, Chem. Listy, 105 (2011) 820-821.

[19] T.B. Massalski, H. Okamoto, P.R. Subramanian, L. Kacprzak, Binary Alloy Phase Diagrams – Vol. 1, ASM International, Ohio, 1990.

[20] G.A. López, S. Somadossi, P. Zieba, W. Gust, E.J. Mittemeijer, Mater. Chem. Phys., 78 (2002) 459-463.

[21] P. Zhu, J.C.M. Li, C.T. Liu, Mater. Sci. Eng., 239-240 A (1997) 532-539.

[22] Y. Li, Y.X. Nan, W.X. Guo, H.Q. Che, Q.C. Fan, Intermetallics, 18 (2010) 179-187.

[23] Y.G. Nakagawa, G.C. Weatherly, Acta Metallurgica, 20 (1972) 345-350.

[24] A. Juarez-Hernandez, H. Jones, Scripta Materialia, 38 (1998) 729-734.

[25] D.H. Pi, J.M. Park, G.A. Song, J.H. Han, K.R. Lim, S. Yi, S.H. Yi, D.H. Kim, N.S. Lee, Y. Seo, K.B. Kim, Intermetallics, 18 (2010) 1856-1859.

[26] H. Bei, E.P. George, E.A. Kenik, G.M. Pharr, Acta Materialia, 51 (2003) 6241-6252.

[27] J.H. Han, G.A. Song, J.M. Park, J.K. Lee, S.Yi, D.H. Kim, K.B. Kim, J. Alloy Compd., 491 (2010) 178-181.